Eur. Phys. J. A **2**, 263–268 (1998)

THE EUROPEAN PHYSICAL JOURNAL A

Effective charges for ^{88}Sr and ^{90}Zr closed-shell cores

I.P. Johnstone, I.S. Towner

Department of Physics, Queen's University, Kingston, Ontario K7L 3N6, Canada

Received: 16 February 1998
Communicated by D. Schwalm

Abstract. Effective charges are calculated for protons and neutrons in the region of mass 90. It is found that their magnitudes differ appreciably depending on whether the proton $p_{1/2}$ shell is empty or full. The calculated values are compared with values deduced from nuclei with simple configurations, and from a fit to N=50 data. The empirical values are used in shell-model calculations of quadrupole moments of N=50-58 nuclei.

PACS. 21.10.Ky Electromagnetic moments – 21.60.Cs Shell model – 27.60.+j $90 \leq A \leq 149$

1 Introduction

The effective charges, $e_{\rm eff}$ (also to be written e_π and e_ν when distinguishing proton and neutron cases), of valence nucleons close to the Fermi surface reflect the polarizing effect the nuclear core has on the properties of valence nucleons. In particular, the E2 giant quadrupole resonance, understood as a coherent superposition of particle-hole states, is a dominating influence. In this work we will use the linked valence cluster theory described by Brandow [1] to evaluate the effective charge, $e_{\rm eff}$, for closed-shell-plus (or minus)-one configurations relative to closed shells at ^{88}Sr and ^{90}Zr. The calculations are carried out to second order in the perturbing interaction.

The most reliable data on $e_{\rm eff}$ are obtained from measurements of static quadrupole moments, Q, of high-spin isomers in nuclei near closed shells, since they have relatively pure shell-model character. For this reason, we will concentrate on Q moments although we will also consider some transition $B(E2)$ values. The first comprehensive study of the $g_{9/2}$ orbital in the A $\simeq$ 90 mass region was given by Raghavan et al. [2]. Our work builds on this start.

In Sect. 2 we give a fully microscopic calculation of $e_{\rm eff}$ for a number of different orbitals in the A $\simeq$ 90 mass region. We will comment, in particular, on the state dependence of the results. In Sect. 3 we compare these results with experimental data in nuclear states whose configurations are likely to be quite pure. More detailed shell-model calculations are given in Sect. 4, which will gauge the success and usefulness of the deduced $e_{\rm eff}$ values.

2 Calculation of effective charges

Consider, by way of an example, the quadrupole moment of the ground state, $5/2^+$, of ^{89}Sr. Naively, this nucleus can be described as a closed shell, ^{88}Sr, plus an additional neutron in the $d_{5/2}$ orbital. Its quadrupole moment is given in terms of a single-particle matrix element multiplied by an effective charge. Of course, describing a nucleus in this way is an extreme case of truncation in the shell-model space. To the extent that the effective residual interaction among nucleons near the Fermi surface is weak, a perturbation expansion can be developed formally [1] to derive an effective operator that can be used in truncated model spaces: $\hat{Q}_{\rm eff} = e_{\rm eff}\hat{Q}$. This, in essence, is the definition of the effective charge and the procedure is completely successful if the single-particle matrix element of $\hat{Q}_{\rm eff}$ reproduces the experimental result.

There have been a number of calculations where $\hat{Q}_{\rm eff}$ has been evaluated to second order [3–7] and to higher orders [6–9], but only in light nuclei. We are not aware of any systematic calculations in medium-mass nuclei. Our methodology closely follows that of Ellis and Siegel [4], where the formal expansion can be represented in terms of a number of Goldstone diagrams. The rules for interpreting these diagrams have been given, for example, in [10]. Briefly an upgoing line represents an orbital unoccupied in the chosen closed-shell core (particle state), while a downgoing line represents an occupied orbital (hole state). We evaluate the diagrams using the harmonic oscillator potential as the one-body Hamiltonian that provides the basis for the calculation; all matrix elements are evaluated in an oscillator basis. It would be preferable to use a Hartree-Fock procedure to provide the mean average field. Ellis and Mavromatis [11] have given all the Hartree-Fock insertion graphs that would enable a calculation in an oscillator basis to be corrected to second order to a Hartree-Fock basis. In this work, however, we have not calculated these Hartree-Fock insertion graphs, arguing that for our purposes an oscillator basis is sufficiently close to a Hartree-Fock basis. It remains to specify the

Table 1. Calculated effective charges in closed-shell-plus (or minus)-one configurations, broken down by class of diagram

	Empty $\pi p_{1/2}$ orbit			Full $\pi p_{1/2}$ orbit		
	$\nu(g_{9/2}^{-1})$	$\nu(d_{5/2})$	$\pi(g_{9/2})$	$\nu(g_{9/2}^{-1})$	$\nu(d_{5/2})$	$\pi(g_{9/2})$
Zeroth order:	0.00	0.00	1.00	0.00	0.00	1.00
First order:	1.01	0.72	0.37	0.67	0.49	0.26
Second order: RPA	0.85	0.63	1.21	0.50	0.35	0.79
Second order: RPA corr.	0.07	0.04	−0.30	0.06	0.02	−0.15
Second order: NCS	0.02	0.02	−0.17	0.01	0.01	−0.17
Second order: Other	0.00	0.00	−0.00	0.00	0.00	0.00
Sum	1.95	1.40	2.12	1.23	0.88	1.72

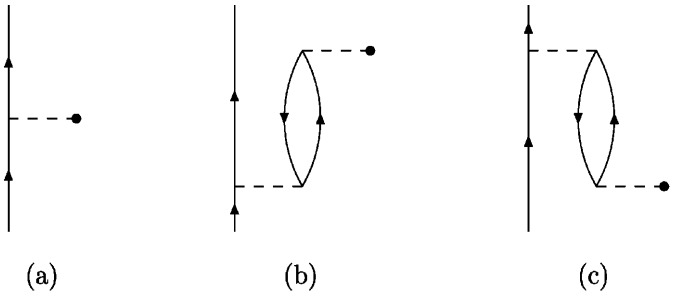

Fig. 1. Zeroth-order and first-order core-polarisation graphs. Diagram **c** is the Hermitian adjoint of diagram **b**

effective residual interaction. We will use a G-matrix constructed from the Paris potential and parameterised as a sum of Yukawa potentials of various ranges and strengths by Hosaka et al. [12].

All the graphs required for the construction of the effective operator, $\hat{Q}_{\rm eff}$, are given in Figs. 1–5. In Fig. 1, diagram (a) is the zeroth-order term; it represents the bare operator, $\hat{Q}$, evaluated between single-particle oscillator states. The effective charge is given by the sum of all other diagrams divided by this zeroth-order term evaluated for a proton. Diagrams (b) and (c) are the only first-order terms; they are known as the core-polarisation graphs and select out just the 2^+ particle-hole components in the residual interaction. We note that the neutron effective charge is twice as big as that for a proton from these graphs. This is evident in Table 1, where we give some results for a neutron in orbitals $g_{9/2}$ and $d_{5/2}$, and a proton in $g_{9/2}$. We consider two cases where the closed shell is considered to be ^{88}Sr or ^{90}Zr. The difference is whether the proton $p_{1/2}$ orbital is empty or full. We return to this point later.

In Fig. 2 are the most important of the second-order graphs. They represent a continuation of 2^+ particle-hole interactions that lead to a start of a geometric series, which if summed to all orders, would be equivalent to a Random Phase Approximation (RPA) calculation. These graphs are in phase with the first-order graphs and give a sizeable contribution to the effective charge, especially for a proton. Note that the sum of first-order and second-order RPA graphs gives an effective charge for a proton almost comparable to that for a neutron. However, the valence particle in these diagrams is not antisymmetrised with respect to the particle line in the second bubble. This is corrected by the series of diagrams shown in Fig. 3, which are known as the RPA vertex-correction graphs. Their contribution to the effective charge is small for neutrons, but of reasonable size for protons, cancelling some of the RPA enhancement.

In Fig. 4 are a number of diagrams in which the one-body operator acts on a particle or hole line as opposed to operating on a particle-hole pair. This set of diagrams is called a 'number-conserving' set (NCS). That is, if the E2 operator is replaced by the number operator, the sum of these graphs would be identically zero. Thus one expects a reasonable degree of cancellation among these graphs. This appears to be so, as the contribution to the neutron effective charge is very small. There remains a reasonable size contribution for protons, but this comes mainly from the folded graphs, which are correcting the normalisation associated with the zeroth-order contribution. These folded graphs give zero contribution to the effective charge of a neutron.

Finally, in Fig. 5 are a number of graphs, which can all be interpreted as a one-body matrix element multiplied by a second-order correction to the single-particle energy of the valence state. These graphs all give a negligible contribution to the effective charge.

This raises the question of the appropriate energy denominators to be used for the intermediate states in the perturbation expansion. Formally, these energies are given in terms of the eigenenergies of the single-particle states of the one-body Hamiltonian, the harmonic oscillator, and so are integral multiples of $\hbar\omega$. We have only kept intermediate states of energy up to $2\hbar\omega$. This is because in first-order graphs, states of $\geq 4\hbar\omega$ energy give zero contribution, a result that follows from the properties of the operator, $\hat{Q}$, and harmonic oscillator functions. However, as the closed-shell cores we are using for these calculations, ^{88}Sr and ^{90}Zr, are jj-closed shells rather than LS-closed shells, we cannot use simple integral multiples of $\hbar\omega$ for the single-particle energies. This is because some of the unoccupied particle orbitals are degenerate with some of the occupied hole orbitals and that could result in certain energy denominators in the perturbation expansion

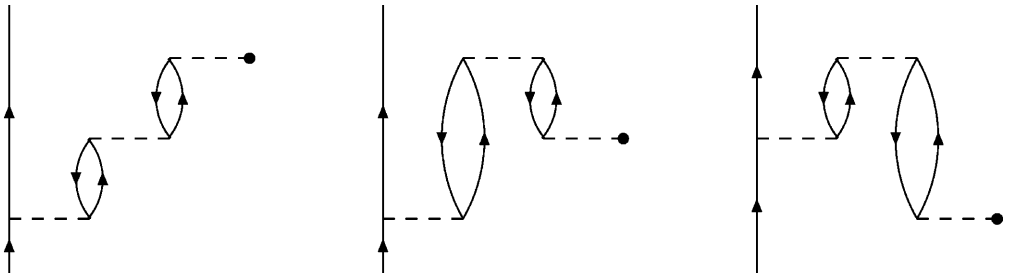

Fig. 2. Second-order graphs contributing to the RPA series. Hermitian adjoint graphs are not shown

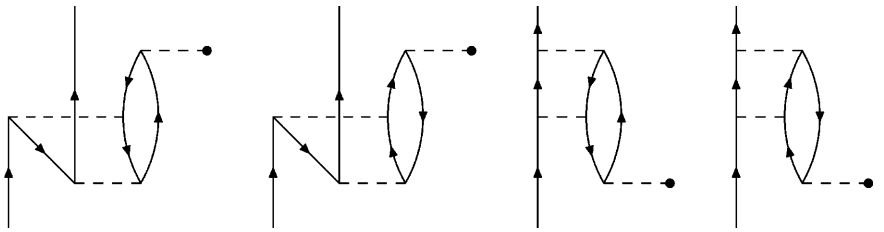

Fig. 3. Second-order graphs representing vertex corrections to the RPA series. Hermitian adjoint graphs are not shown

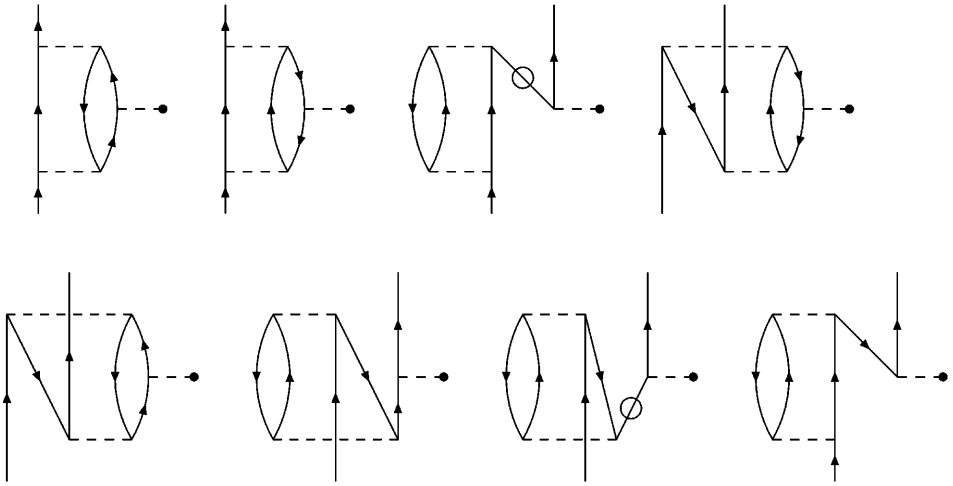

Fig. 4. Second-order graphs representing the number-conserving sets. Lines with a 'loop' on them are folded lines [1] and represent normalisation-correction graphs. Hermitian adjoint graphs are not shown

becoming zero. Of course, it is the spin-orbit force that splits this degeneracy and in medium-mass nuclei the contribution of the spin-orbit force to level spacing is very important. Therefore, following Bohr and Mottelson [13], we add to the one-body oscillator the terms

$$v_{ls}\hbar\omega(\mathbf{l}.\mathbf{s}) + v_{ll}\hbar\omega\left(\mathbf{l}^2 - \langle\mathbf{l}^2\rangle_N\right), \tag{1}$$

$$\langle\mathbf{l}^2\rangle_N = \frac{1}{2}N(N+3), \tag{2}$$

where $N = 2n+l$ is the principal quantum number for the oscillator orbital, n the number of radial nodes (excluding the origin and infinity) and l the orbital angular momentum quantum number. There is no radial dependence to these terms, so the eigenfunctions remain oscillator functions, but the degeneracy among the single-particle energies is removed. We use the values $v_{ls} = -0.127$ and $v_{ll} = -0.03$ from [13]. We make a further fine adjustment to these energies for the single-particle states close to the Fermi surface so that they match exactly experimental values determined in pickup and stripping reactions. The values of the single-particle energies used are given in Table 2.

Table 2. Single-particle energies for neutrons and protons near the Fermi surface from pick-up and stripping reaction data. All other single-particle energies are given by $N\hbar\omega$ plus a spin-orbit shift from (1) and normalised to the $1d_{5/2}$ value for neutrons and to the $1p_{1/2}$ value for protons

	Neutron	Proton
$1p_{3/2}$	−15.14	−10.61
$0f_{5/2}$	−14.98	−11.03
$1p_{1/2}$	−11.50	−7.12
$0g_{9/2}$	−11.11	−6.25
$1d_{5/2}$	−6.36	−2.38
$2s_{1/2}$	−5.33	−0.47
$1d_{3/2}$	−4.35	−0.39
$0g_{7/2}$	−3.69	−0.69

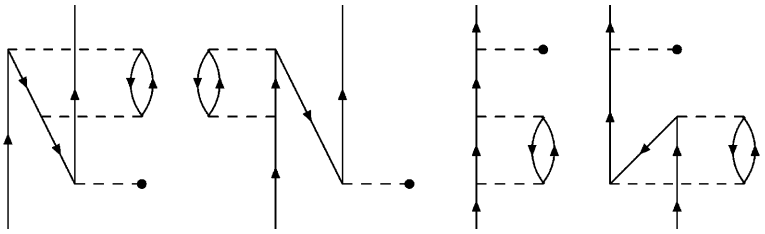

Fig. 5. Second-order graphs that effectively modify the single-particle energy of the valence orbital. Hermitian adjoint graphs are not shown

Table 3. Calculated effective charges in closed-shell-plus (or minus)-one configurations

Orbit	Empty $\pi p_{1/2}$ orbit	Full $\pi p_{1/2}$ orbit
Diagonal		
$\nu g_{9/2}^{-1}$	1.95	1.23
$\nu g_{7/2}$	1.92	1.26
$\nu d_{5/2}$	1.40	0.88
$\nu d_{3/2}$	1.35	0.87
$\pi g_{9/2}$	2.12	1.72
Off-diagonal		
$\nu g_{7/2} - \nu d_{5/2}$	1.31	0.93
$\nu g_{7/2} - \nu d_{3/2}$	1.20	0.91
$\nu d_{5/2} - \nu d_{3/2}$	1.40	0.93
$\nu d_{5/2} - \nu s_{1/2}$	1.08	0.79
$\nu d_{3/2} - \nu s_{1/2}$	1.03	0.77

Returning to Table 1, we see the summed result for the effective charge depends quite critically on whether the closed-shell core is taken to be ^{88}Sr (the proton $p_{1/2}$ orbit empty) or ^{90}Zr (the proton $p_{1/2}$ orbit full). The reason is that in the first case there are first-order contributions to the effective charge arising from $\Delta N = 0$ particle-hole excitations, $\pi(p_{1/2}, p_{3/2}^{-1})$ and $\pi(p_{1/2}, f_{5/2}^{-1})$. In the second case these contributions are absent. Thus in shell-model calculations it is important to use different effective charges for the two cases. This was first stressed by Raghavan et al. [2].

In Table 3 we give the summed result for the effective charge from second-order calculations for a number of orbitals relative to the two closed shells, ^{88}Sr and ^{90}Zr. Both diagonal and off-diagonal matrix elements are listed. Notice there is some state-dependence evident in the results. Orbitals with a smaller orbital angular momentum, l, have a smaller calculated effective charge.

3 Comparison with data for simple configurations

To get a quick estimate of how successful these effective-charge calculations are, we consider experimental data for nuclei that can be considered predominantly closed-shell-plus-one configuration, or closed-shell-plus-n, where n is a small number. We will not consider any variation of the effective charge with n. The best cases are the quadrupole moments of the ground states of ^{87}Sr and ^{89}Sr, which lead almost directly to the effective charge of a $\nu g_{9/2}^{-1}$ hole orbital and a $\nu d_{5/2}$ particle orbital relative to a ^{88}Sr core. The result is shown in Table 4. For neutrons relative to a ^{90}Zr core, there is no good experimental datum to provide a value for $e_\nu(g_{9/2}^{-1})$, while the quadrupole moment of the ground state of ^{91}Zr should provide $e_\nu(d_{5/2})$. However, in the latter case shell-model calculations, to be discussed in Sect. 4, suggest this is not a good single-particle state but has a mix of configurations with the proton $p_{1/2}$ orbit empty and configurations with the proton $p_{1/2}$ orbit fully occupied. An effective charge derived from ^{91}Zr would therefore be interaction-dependent. A better approach is to use the quadrupole moment of the 2^- state in ^{90}Y, which should have a rather pure $p_{1/2}d_{5/2}$ configuration. This gives $e_\nu(d_{5/2}) = 1.36$ when the proton $p_{1/2}$ shell is half filled, and when combined with the value of $e_\nu(d_{5/2}) = 2.05$ for a ^{88}Sr core suggests that the value of $e_\nu(d_{5/2})$ for a ^{90}Zr core should be about 0.67.

For the proton effective charges, we have carried out a least-squares fit to 15 quadrupole moments and $B(E2)$ values of N=50 nuclei, using the model space and interaction of Gloeckner and Serduke (GS) [14]. Data were weighted with experimental uncertainties, with the minimum uncertainty set equal to 10% of the average quadrupole reduced matrix element. The rms error of this fit, the results of which are given in Table 4, was significantly lower ($\chi = 0.91$ rather than $\chi = 1.55$) than for a fit (giving $e_\pi(g_{9/2}) = 1.77$), which assumed equal effective charges for ^{88}Sr and ^{90}Zr cores.

In general, the comparison between theory and experiment seems to be very good for the $g_{9/2}$ orbital for both protons and neutrons, for both cores considered. The same, however, cannot be said for neutrons in the $d_{5/2}$ orbital. For a ^{88}Sr core, the theory is underpredicting, while for a ^{90}Zr core, the theory overpredicts. Indeed, the massive change indicated by experiment in $e_\nu(d_{5/2})$ between ^{88}Sr and ^{90}Zr cores is going to be very difficult to understand. This difference is dominated by the calculation of the first-order core-polarisation graphs as discussed in Sect. 2, and the contribution from these graphs would have to be doubled to fit this result. That would imply a doubling of the strength of the Paris G-matrix interaction in this 2^+ particle-hole channel. Such a doubling, however, would seriously damage the agreement already achieved between theory and experiment for the g orbits. Therefore this result poses a puzzle.

4 Shell-model calculations

Quadrupole moments are calculated here for N=50-58 nuclei using the proton effective charges derived from

Table 4. Comparison of computed effective charges with experimental values deduced from closed-shell-plus-one nuclei, or other states with simple configurations

Orbit	Empty $\pi p_{1/2}$ orbit	Full $\pi p_{1/2}$ orbit
$\nu(g_{9/2}^{-1})$	^{87}Sr: $Q = +0.355(20)$ e · b Expt: $e_\nu = 1.87 \pm 0.01$ Theory: $e_\nu = 1.95$	Theory: $e_\nu = 1.23$
$\nu(d_{5/2})$	^{89}Sr: $Q = -0.291(15)$ e · b Expt: $e_\nu = 2.05 \pm 0.11$ Theory: $e_\nu = 1.40$	^{90}Y: $Q(2^-) = -0.155(3)$ e · b Expt: $e_\nu = 0.67 \pm 0.15$ Theory: $e_\nu = 0.88$
$\pi(g_{9/2})$	Fit to 15 data in N=50 nuclei Fit: $e_\pi = 2.11 \pm 0.09$ Theory: $e_\pi = 2.12$	Fit to 15 data in N=50 nuclei Fit: $e_\pi = 1.60 \pm 0.06$ Theory: $e_\pi = 1.72$

Table 5. Quadrupole moments (in units of e · b) calculated in the shell model in three different model spaces and compared with experiment [18]

		Model Space			
Nucleus	Experiment	(1)	(2)	(3)	(3′)
^{90}Zr(8^+)	−0.51(3)	−0.51			
^{91}Zr($5/2^+$)	−0.206(10)	−0.20	−0.20	−0.22	−0.20
^{91}Zr($21/2^+$)	(−)0.86(5)	−0.81	−0.81	−0.81	−0.72
^{93}Nb($9/2^+$)	−0.32(2), −0.366(18)	−0.35	−0.38	−0.39	−0.38
^{92}Mo(8^+)	±0.34	−0.34			
^{94}Mo(2^+)	−0.13(8) or +0.01(8)	0.21	0.19	−0.05	−0.02
^{94}Mo(8^+)	±0.47(1)	−0.43	−0.46	−0.45	−0.47
^{95}Mo($5/2^+$)	−0.022(1)	0.03	0.01	−0.05	−0.04
^{96}Mo(2^+)	−0.20(8) or +0.04(8)	−0.06	0.00	−0.14	−0.11
^{97}Mo($5/2^+$)	+0.17(4)	0.26	0.21	0.29	0.27
^{98}Mo(2^+)	−0.26(9) or +0.10(9)	0.17	0.19	0.26	0.26
^{100}Mo(2^+)	−0.39(8) or −0.13(8)		0.14	−0.18	−0.13
^{99}Tc($9/2^+$)	−0.129(6)	−0.11	−0.12	−0.13	−0.17
^{96}Ru(2^+)	−0.13(9)	0.16	0.10	−0.14	−0.13
^{98}Ru(2^+)	−0.20(9) or −0.01(9)	−0.11	0.03	−0.18	−0.17
^{99}Ru($5/2^+$)	+0.079(4)	0.30	0.10	0.26	0.27
^{99}Ru($3/2^+$)	+0.231(12)	0.02	−0.15	−0.16	−0.17
^{100}Ru(2^+)	−0.43(7) or −0.20(7), −0.13(7)	0.04	−0.07	−0.06	−0.05
^{101}Ru($5/2^+$)	+0.457(23)		0.41	0.49	0.47
^{102}Ru(2^+)	−0.57(7) or −0.35(7)		0.00	−0.26	−0.24
^{102}Pd(2^+)	−0.20(15)	−0.09	−0.20	−0.26	−0.27
^{104}Pd(2^+)	−0.46(10)		−0.13	−0.22	−0.22
^{103}Cd($5/2^+$)	−0.79(66)	0.23	−0.03	0.06	0.07
^{105}Cd($5/2^+$)	+0.43(4)		0.26	0.30	0.33
^{106}Cd(2^+)	−0.28(8) or −0.12(8)		−0.20	−0.10	−0.10
^{104}In(5^+)	+0.66(11)	0.14	0.36	0.23	0.27
^{105}In($9/2^+$)	+0.83(5)	0.30	0.39	0.42	0.50

the N=50 least-squares fit (1.60 and 2.11 for filled and empty $p_{1/2}$ shell), and orbit-independent neutron effective charges set equal to the empirical $d_{5/2}$ values (0.67 and 2.05 for filled and empty proton $p_{1/2}$ shell). In all calculations protons were allowed to span the $p_{1/2}$ and $g_{9/2}$ shells. For N=50, the interaction was that of GS [14], which was fitted to spectra of N=50 nuclei, while for N=51-58 three different neutron model spaces were used. In model space (1) neutrons were restricted to the $d_{5/2}$ shell, and the neutron-proton interaction, taken from [15], was from a fit to spectra of N=51 nuclei. The neutron-neutron interaction was a set of $d_{5/2}^2$ matrix elements chosen to optimize the calculated binding energies for the Zirconium isotopes. In model space (2) the neutrons are restricted to the $d_{5/2}$ and $s_{1/2}$ shells. The interaction was that of Gloeckner [16], which was derived from a fit to levels of Zirconium and Niobium isotopes. Finally, in model space (3) the neutrons are distributed among the $d_{5/2}$, $s_{1/2}$, $d_{3/2}$ and $g_{7/2}$ shells but with the restriction that no more than two neutrons be taken out of the $d_{5/2}$ shell. The interaction was

the JS6 interaction of Johnstone and Skouras [17], which has proton-proton and proton-neutron components similar to those of model space (1). The neutron-neutron interaction is a volume delta force, with the important $d^2_{5/2}$ matrix elements chosen to reproduce the ^{92}Zr spectrum. The calculated quadrupole moments for a range of nuclei with mass number A between 90 and 105, evaluated with these interactions, are given in Table 5.

Quadrupole moments of 2^+ states differ appreciably in the three model spaces. Model space (3) gives the best agreement with experiment, tending to give the negative moments required empirically. The magnitudes of the calculated moments are too small for several of the higher-mass isotopes. We also give a second calculation, based on model space (3), but using this time the calculated effective charges from Table 3 rather than the empirical ones. This calculation, labelled (3′) in Table 5, does not differ very much from that labelled (3).

5 Summary

Effective charges have been calculated for protons and neutrons in the region of mass 90, and compared with empirical values deduced from experimental data. Calculated and empirical values are in close agreement for protons, but there is less satisfactory agreement for neutrons. Theory predicts that the effective charges depend strongly on whether the proton $p_{1/2}$ shell is full or empty, and a least-squares fit to quadrupole data of N=50 nuclei appears to confirm this. Quadrupole moments have been calculated for a wide range of nuclei using three different model spaces for neutrons.

References

1. Brandow, B.H.: Rev. Mod. Phys. **39**, 771 (1967)
2. Raghavan, P., Senba, M., Ding, Z.Z., Lopez-Garcia, A., Brown, B.A., Raghavan, R.S.: Phys. Rev. Lett. **54**, 2592 (1985)
3. Siegel, S., Zamick, L.: Nucl. Phys. **A145**, 89 (1970)
4. Ellis, P.J., Siegel, S.: Phys. Lett. **34B**, 177 (1971)
5. Barrett, B.R., Kirson, M.W.: Nucl. Phys. **A148**, 145 (1970)
6. Kirson, M.W.: Ann. of Phys. **66**, 624 (1971); Kirson, M.W.: Ann. of Phys. **68**, 556 (1971); Kirson, M.W.: Ann. of Phys. **82**, 345 (1974)
7. Ellis, P.J., Osnes, E.: Rev. Mod. Phys. **49**, 777 (1977)
8. Krenciglowa, E.M., Kuo, T.T.S., Osnes, E., Ellis, P.J.: Nucl. Phys. **A289**, 111 (1977)
9. Chakravarti, S., Ellis, P.J., Kuo, T.T.S., Osnes, E.: Phys. Lett. **B109**, 141 (1982)
10. Towner, I.S.: A shell model description of light nuclei. Oxford: Clarendon Press 1977
11. Ellis, P.J., Mavromatis, H.A.: Nucl. Phys. **A175**, 309 (1971)
12. Hosaka, A., Kubo, K.-I., Toki, H.: Nucl. Phys. **A444**, 76 (1985)
13. Bohr, A., Mottelson, B.R.: Nuclear structure. vol. 2. New York: Benjamin 1975
14. Gloeckner, D.H., Serduke, F.F.D.: Nucl. Phys. **A220**, 477 (1974)
15. Johnstone, I.P., Phys. Rev. **C44**, 1476 (1991)
16. Gloeckner, D.H., Nucl. Phys. **A253**, 301 (1975)
17. Johnstone, I.P., Skouras, L.D.: Phys. Rev. **C51**, 2817 (1995)
18. Raghavan,P.: Atomic Data and Nuclear Data Tables, **42**, 189 (1989)